Ain Shams University
Faculty of Education
Chemistry Department

Role of dominated rutile/anatase ratio of $H_3PMo_{12}O_{40}/TiO_2$ for physicochemical characterization and photocatalytic studies

تأثير نسبة الروتايل إلى الاناتيز ل $H_3PMo_{12}O_{40}/TiO_2$ على الخصائص الفيزيائية الكيميائية و دراسات النشاط الضوئى الحفزى

رسالة مقدمة من

حنان عاطف سليمان عبيد

بكالوريوس في العلوم والتربية
(كيمياء) ٢٠١١ م

للحصول على درجة الماجستيرلإعداد المعلم في العلوم
(كيمياء فيزيائية)

تحت إشراف

د.ليلى ابراهيم على
أستاذ الكيمياء الفيزيائية المساعد – كلية التربية- جامعة عين شمس

د. مني مصطفي على سيف
أستاذ الكيمياء غير العضوية المساعد – كلية التربية- جامعة عين شمس

د. مروه محمد ابراهيم
مدرس الكيمياء الفيزيائية – كلية التربية- جامعة عين شمس

Role of dominated rutile/anatase ratio of $H_3PMo_{12}O_{40}/TiO_2$ for physicochemical characterization and photocatalytic studies

Hanan A. Soliman, Laila I. Ali, Marwa M. Ibrahim, M. Saif*

Department of Chemistry, Faculty of Education, Ain Shams University, Roxy, 11711, Cairo, Egypt

*Corresponding author: email: mona_saif1@yahoo.com; Phone No. 0201009642295; Fax. (02) 22581243

Abstract

The effect of phosphomolybdic acid ($H_3PMo_{12}O_{40}$; PMo_{12}) on structural, surface, morphology, optical as well as photoluminescence and photocatalytic properties of TiO_2 prepared by sol-gel method under template-free condition has rarely been reported. The present work has found that the content of different PMo_{12} manipulated of TiO_2 crystal phase (rutile/anatase ratio). The TEM analysis confirms the formation of titania mesoporous in the presence of PMo_{12}. The increasing of PMo_{12} contents significantly increased the TiO_2 surface area and decreased of crystal size as a result of introducing of kegging unit. The PMo_{12} contents were not only controlled the crystal and surface properties of TiO_2 nanoparticles but also were controlled the optical properties also. The UV–Vis light reflectance spectra and PL emission of PMo_{12} doped TiO_2 were blue shifted in as compared to pure TiO_2 nanoparticles. The photoluminescence measurements for pure and PMo_{12} doped TiO_2 confirm that PMo_{12} significantly decrease the electron–hole recombination chance in the obtained TiO_2. The photo-oxidative activity of different PMo_{12} doped TiO_2 mesoporous was evaluated using new fluorescent probe and dye methods. Moreover, the effect of different calcination temperatures and time during preparation on physicochemical properties of PMo_{12} doped TiO_2 were also studied.

Keywords: Mesoporous materials; Heterogeneous catalysis; Environmental chemistry; Fluorescent probe; optical properties

1. Introduction

Advanced photochemical oxidation (APO) considered a one of the important technologies for treatment of contaminated water, air, and solids. Nano-semiconductors are used to destroy environmental contaminants. The metal oxides are considered as efficient examples of semiconductors and their reaction takes place by light-induced redox reactions and generation of conduction band electrons and valence band holes. A wide range of metal oxides may be used for semiconductor-sensitized processes, such as TiO_2, ZnO, MgO, WO_3, Fe_2O_3 and CdS [1, 2].

TiO_2 is mostly chosen in APO process due to its high photoconductivity and photostablity in solution, ready availability, low toxicity, low cost, a large band gap of 3.2 eV, higher electron mobility, low dielectric constant and lower density [3, 4]. For these reasons, several heterogeneous applications have been reported at the interface of illuminated TiO_2 photocatalyst like environmental cleanup, self-cleaning, antimicrobial surfaces, sterilization and hydrogen evolution [5-9]. Rutile, anatase and brookite are the most important three crystalline forms of TiO_2 [8, 10]. Rutile is the thermodynamically stable state, whereas the other two phases are metastable. Anatase and brookite structures transformed to the rutile phase after reaching a certain particle size. So phases of TiO_2 are considered the critical parameter which determines the activity of TiO_2 [8, 11].

TiO_2 suffers from several limitations like the high electrons and holes recombination ratio on the TiO_2 surface under ultraviolet illumination and null photoresponse of TiO_2 under visible light irradiation [4]. These limitations can

be overcome by preparation method and dopping with different materials [3, 4, 8, 12]. The used methods to overcome the limitations of TiO_2 effect on crystal size, phase type, morphology and a phase-dependent synergistic effect. A phase-dependent synergistic effect means that photo-excited electrons in the conduction band (CB) of one polymorph of TiO_2 migrate across the phase boundary to the CB of the other [13-20].

polyoxometallates (POMs, molecular metal oxide anions) is considered one of dopant materials supported on TiO_2. Heteropolyacids (HPA), such as $H_3PMo_{12}O_{40}$ (PMo_{12}) is considered as a kind of widely used POMs which is very strong BrØnsted acids and efficient oxidants that perform fast and reversible redox multielectron transformations under mild conditions. It can act as bifunctional catalyst used in solution as acid and oxidation catalyst. Also, it has well defined structure and properties and its size is typically a few nanometers [3, 4, 12]. Unfortunately, PMo_{12} as one of HPAs is soluble in aqueous solution and cannot be separated for recovery. So, incorporation of HPA (PMo_{12}) into TiO_2 has attracted much attention since the support makes HPA easily recycled. In the HPA-TiO_2 system, the synergistic effect originates from the interfacial electron transfer from TiO_2 conduction band to HPA (PMo_{12}) after UV irradiation. Such effective electron transfer can inhibit fast electron - hole recombination in TiO_2, and the trapped holes have sufficient time to react with H_2O to generate $^{\bullet}OH$ radicals which degraded the dye solution [4].

Most of published research focused on preparation of HPA modified titania by different methods such as sol-gel and hydrothermal in the presence of template for different photocatalytic studies [4, 16, 22, 25-26]. However, the effect of heteropolyacids on structural, surface, morphology, optical as well as

photoluminescence and photocatalytic properties of TiO_2 prepared by sol-gel method under template-free condition has rarely been reported.

In this work, PMo_{12} as one of heteropolyacids - controlled titania nanostructure properties was synthesized by sol-gel method in the absence of any template. The effect of PMo_{12} on different physicochemical properties of titania like structural, surface, morphology, optical and photoluminescence were investigated under different conditions. The photocatalytic activity of PMo_{12} modified titania nanostructure was evaluated using new fluorescent probe method and dye method.

2. Experimental

2.1. Materials and reagents

The chemicals used for preparation of catalysts were used as received and there were of analytical grade. Titanium tetraisopropoxide (TTIP), Ti $[O(C_3H_7)]_4$ was purchased from ACROS (USA). Phosphomolybdic acid hydrate (PMo_{12}), $H_3PMo_{12}O_{40}.24H_2O$ was supplied from ALPHA CHEMIKA and was as extra pure. Nitric acid (96%) was purchased from Merck (Germany). Coumarin $C_9H_6O_2$ was obtained from Aldrich. 7-hydroxycoumarin $C_9H_6O_3$ was obtained from ACROS ORGANICS. Bi-distilled water was used. The Remazol Red RB-133 dye (Reactive Red RB 133, RR) was obtained from DyeStar. The molecular structure of the dye is given in Figure 1.

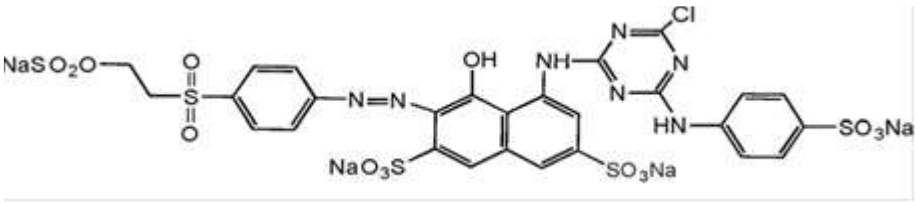

Figure 1: The molecular structure of Ramazol Red RB-133.

2.2. Sol gel preparation method for x-PMo_{12}/TiO_2

Different nano-photocatalysts PMo_{12}/TiO_2 with different contents of PMo_{12} (0.0020, 0.0025, 0.0050, 0.0070, 0.0100, 0.0150 and 0.0200 mol) were prepared by sol gel method as following: Titanium tetraisopropoxide (TTIP, 2.5 mL) were dissolved in 50 ml acidified aqueous solution (pH≈1±0.02), which added dropwise under vigorous stirring in an ice bath for 45 minutes till a clear solution was obtained. Then PMo_{12} was added to the above solution under vigorous stirring. The obtained clear solution was stirred for 4h at 80°C. The resulting semitransparent colloidal suspension solution was evaporated at 80°C to get a powder. The powder was calcinated at 450°C for 1 hour. For comparison, pure TiO_2 was also prepared in the same way without doping by HPA. In the meantime, the effect of calcination temperature (400, 450 and 500°C for 1h.) and calcination time (1, 2 and 3h at 450°C) were studied for 0.0050 PMo_{12}/TiO_2 only.

2.3. Characterization

The crystal properties were investigated by X-ray diffraction (XRD) (a Bruker AXS D8 Advance diffractometer equipped with a graphite monochromator). The surface analysis was measured by a QuantachromeTouchWin™ version 1.11, (USA). The FT-IR spectra of the photocatalysts were recorded using Nicolet IS10 FT-IR 430 spectrometer (USA). UV–vis absorbance and diffuse reflectance spectroscopy (UV–vis/DR) was measured on JASCO V-550 spectrometer (Japan) equipped with an integrating sphere accessory for diffuse reflectance spectra. Barium sulfate was used as a reference in case of diffuse reflectance measurements. Illumination of the prepared photocatalyst were carried out using UV photoreactor (Photon Co., Egypt), in the range from 320 to 410 nm and the intensity of UV radiation is

0.768 mW/cm^2. LS55 spectrofluorometer (Perkin Elemr, USA) used to measure the active oxidative species hydroxyl radicals ($^{\bullet}$OH) produced during the photocatalytic reaction.

2.4. Evaluation methods of photocatalytic activity

Fluorescent probe and dye degradation are the famous methods which used to evaluate the photocatalytic activity of prepared nano-photocatalysts.

2.4.1. Fluorescent probe method for determination of $^{\bullet}$OH radicals

Evaluation of the photo-oxidative activity of the prepared nano-powders using fluorescent probe method was carried out as follows: 0.1 g of photocatalyst was added to acidified aqueous coumarin solution (1.0×10^{-3} M; pH = 3) and illuminated with UV light under vigorous stirring. The fluorescence spectrum (λ_{ex} = 332 nm) for the solution was measured every 10 min of illumination. The concentrations of 7-hydroxycoumarin were specified using a calibration curve based on fluorescence intensity at λ_{max}= 480 nm versus 7-hydroxycoumarin concentration. The apparent rate constant was calculated using the slope of the fluorescence concentration–illumination time curves. They can indirectly represent the apparent rate constant, but not the real values of the rate constant. It should be noted that the blank experiment at the same conditions but without photocatalyst was carried out, which showed that the coumarin without photocatalyst nanoparticles was totally inactive under UV illumination.

2.4.2. Dye method for degradation of RR

This method was carried out as following: 0.1 g of photocatalyst into 100 ml acidified dye solution (5×10^{-5} M, pH $\approx$ 3). The dye solution is stirred in the

dark for 15 min. after the addition of catalyst to establish an adsorption / desorption equilibrium. Samples of suspension are withdrawn every 2.5 min for 30 min. from illumination and are immediately centrifuged at 4500 rpm for 15 min to complete the elimination of catalyst particle. The decolorization efficiency of the studied dye using HPA/TiO_2 at time t, can be expressed as

$$\text{Decolorization efficiency} = 100 \times (A_i - A_f) / A_i \quad (1)$$

where A_i and A_f are the initial and final absorbance values of the dye solution [17, 21].

3. Results and discussion

3.1. Characterization of prepared nano-photocatalyst

3.1.1. XRD

XRD was used to investigate the phase structure and the crystallite size of the as- prepared nanoparticles. Figure 2 shows XRD patterns of pure TiO_2 and PMo_{12}/TiO_2 with different contents of PMo_{12} (0.0025, 0.0050, 0.0070 and 0.0100). Crystal parameters of nanocatalysts were listed in Table 1. All samples showed well-indexed anatase phase (JCPDS 21- 1272) with the diffraction peaks at 25.3°(101), 37.9°(103, 004, and 112), 48.1°(200), 54.4°(105, 211), 62.7°(204) and 69.0°(116,220) [22]. Beside anatase phase, only 0.0050 PMo_{12} / TiO_2 sample contain small amount of rutile phase (JCPDS 21-1276) with the diffraction peaks at 27.5°(110), 36.1°(101) and 41.3°(200) [3, 23]. No diffraction lines attributed to the crystalline PMo_{12} or its decomposition products were observed, indicating that PMo_{12} has been highly dispersed on the support [4, 13, 24-26]. The full width at half maximum (FWHM) increased and the crystal size decreased by increasing doping concentration (Figure 2 and Table 1).

Also, the analytical results showed that the relative intensity of anatase to rutile phases of TiO_2 depending on the content of PMo_{12}. The ratio of the rutile

(110) peak at 27.3° 2θ to anatase (101) peak at 25.3° 2θ was calculated by Spurr and Myers method from the following formula $W_R/W_A=1.22(I_R/I_A)-0.028$, Where W_R and W_A are weight fractions of rutile and anatase, respectively and I_R/I_A is the ratio of the intensities of (110) and (101) peaks [8, 27]. For pure TiO_2, the W_R/W_A equal 0.73. This means that the amount of anatase is higher than that of rutile by 0.2. While W_R/W_A ratio is equal 0.21 for 0.0050 PMo_{12}/TiO_2, due to A – R transformation (Table 1). This means that PMo_{12} act as strong inhibitor for titania phase transformation because of rutile phase disappearance in the others samples.

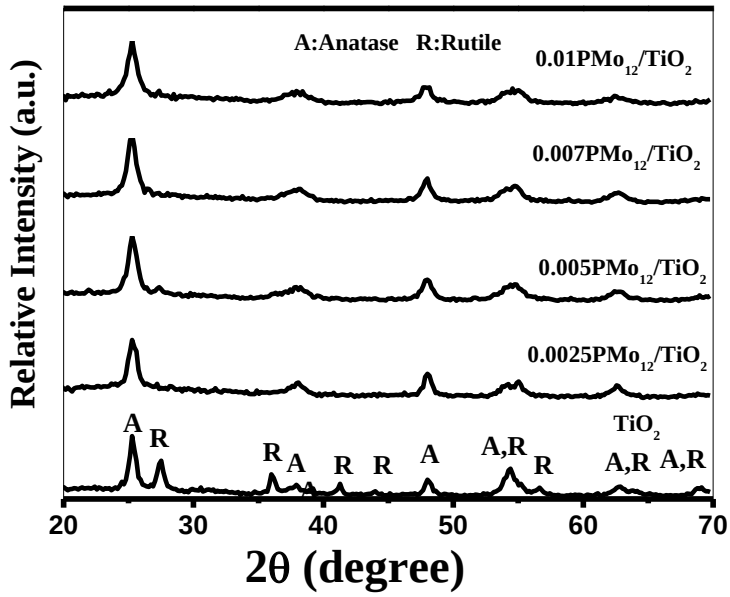

Figure 2: XRD patterns of TiO_2 with different contents of PMo_{12} (0.000, 0.0250, 0.0050, 0.0070, and 0.0100).

3.1.2. Surface area measurements

The textural properties of as prepared TiO_2 and PMo_{12}/TiO_2 nanoparticles with different contents of PMo_{12} were evaluated by the nitrogen sorption determination (Figures 3). From Figures 3, it can be seen that the isotherms belong to type IV according to the IUPAC classification and the result indicates that all samples mainly possess mesoporosity [13, 16, 25, 26]. Table 1 shows the specific surface area S_{BET}, monolayer volume (V_m), total pore volume V_P, average pore radius (**r′**) and mean pore diameter obtained from the N_2 adsorption desorption isotherms and pore size distributions of nanopowders. S_{BET}, V_m and V_P of all doped TiO_2 nanoparticles are higher than undoped one. This is attributed to introducing of kegging unit accompanied by dopping. For 0.0500 PMo_{12}/TiO_2, it has a smallest S_{BET} and crystal size compared to other PMo_{12} contents because of its containing anatase and rutile phases (presence of rutile phase is accompanied by decreasing in S_{BET} [16]). So absence of rutile phase is accompanied by increase in S_{BET} [16]. The average values of pore radius (r′) appear similar for all samples and not much higher than 5.5 nm, indicating that most porosity is due to very small cavities, with size near the boundary of micro and mesopores.

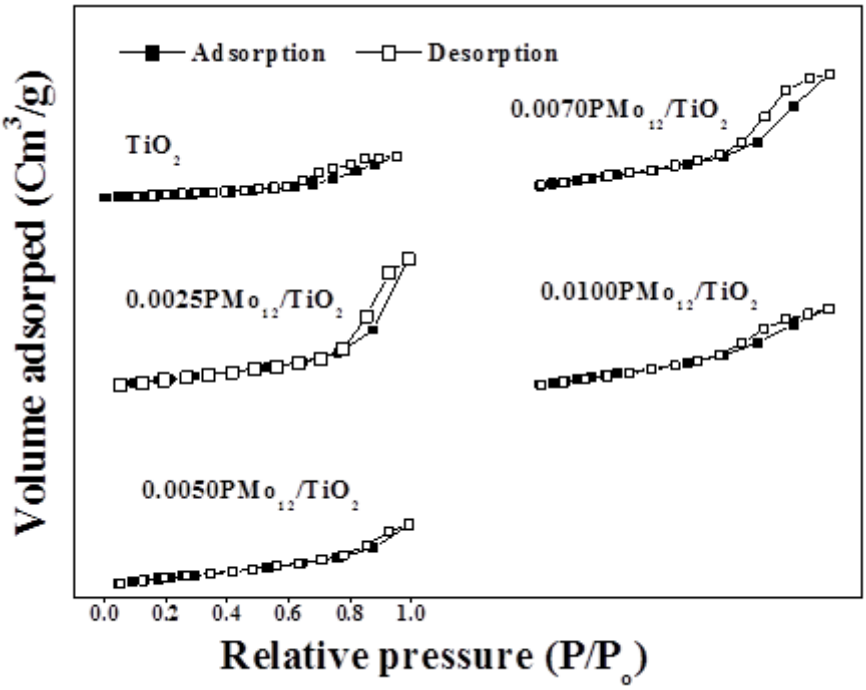

Figure 3: Nitrogen adsorption–desorption isotherms TiO_2 with different contents of PMo_{12} (0.000, 0.0250, 0.0050, 0.0070 and 0.0100).

Additionally, from BJH desorption pore distribution curves, the pure TiO_2 has relatively broad distribution in the meso range with maximum pore diameter of 3.2 nm. PMo_{12}/TiO_2 with different contents have broad distribution from micro to meso range with maximum pore diameter around 1.9 nm in most prepared samples (Table 1, Figures 4).

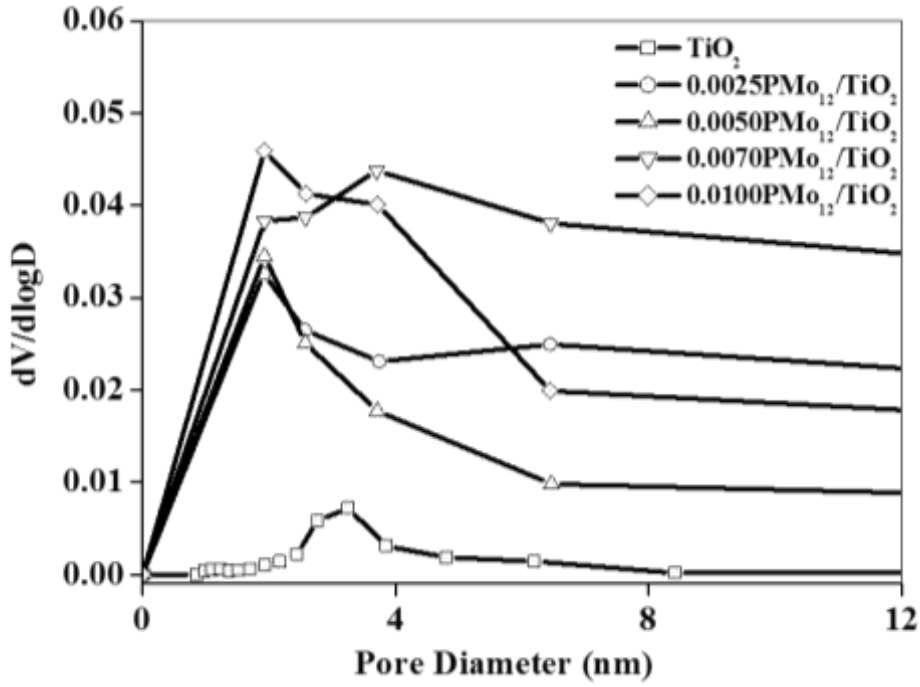

Figure 4: Pore size distribution of TiO_2 with different contents of PMo_{12} (0.000, 0.0050, 0.0070, 0.0100, 0.0150 and 0.0200).

Table 1: XRD analysis and surface properties of PMo_{12}/ TiO_2 nanoparticles.

Sample	L(nm)		FWHM		W_R/W_A	SBET (m^2/g)	V_m (cm^3/g)	V_p (cm^3/g)	r′ (nm)	Mean pore diameter (nm)
	A	R	A	R						
TiO_2	14.05	15.92	0.572	0.507	0.732	58.375	0.017	0.014	4.939	3.245
0.0025 PMo_{12}	11.76	---	0.684	---	---	153.242	0.044	0.427	5.577	1.906
0.0050 PMo_{12}	10.50	18.23	0.765	0.443	0.213	141.029	0.040	0.220	3.119	1.926
0.0070 PMo_{12}	7.92	---	1.015	---	---	168.648	0.048	0.276	3.280	1.924
0.0100 PMo_{12}	5.42	---	1.483	---	---	173.183	0.049	0.390	4.508	2.773

3.1.3. FT-IR

FTIR spectra of pure TiO_2 and PMo_{12}/TiO_2 with different contents were shown in Figure 5. For pure TiO_2, there are three main bands at 3418 cm^{-1}, 1630 cm^{-1} and 530.9 cm^{-1} assigned to stretching vibration of different surface hydroxyl groups (free or bounded), molecular water and the absorption of titania, respectively [26]. In the spectra of PMo_{12}/TiO_2 with different contents of PMo_{12}, the bands attributed to the Keggin's unit skeletal vibrations (1064 cm^{-1}, 975 cm^{-1}, 870 cm^{-1} and 810 cm^{-1} for P- O_a, Mo=O_d, Mo-O_b-Mo and Mo-O_C-Mo, respectively [29]) did not become more intense and they are difficulty noticed implying strong interaction between the Keggin's unit and TiO_2 support at the interface of the two components. Also there are somewhat shifts of the frequencies due to the formation of Mo-O-Ti covelant bonds derived from the interactions between the terminal Mo=O bonds within Keggin units and the surface Ti-OH groups within TiO_2 matrix (Figure 5).

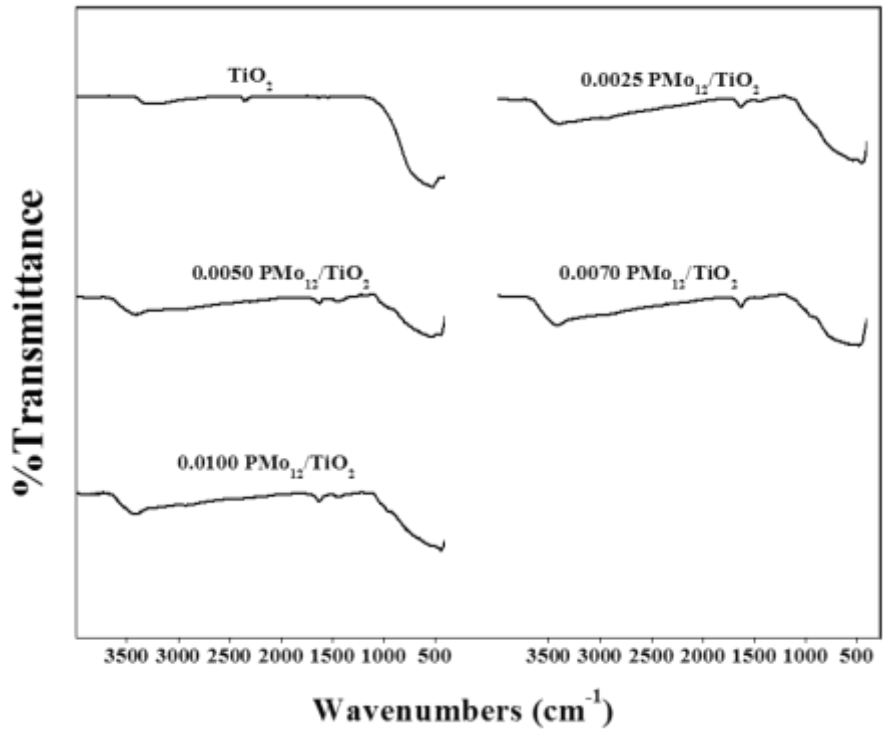

Figure 5: FTIR spectra of pure TiO_2 and PMo_{12}/TiO_2 with different contents of PMo_{12} (0.0050, 0.0070, 0.0100, 0.0150 and 0.0200).

3.1.4. UV-Vis diffuse reflectance and band gap analysis

The effects of different preparation conditions (PMo_{12} concentration and calcination temperature and time) on the optical absorption properties of TiO_2 nanoparticles were studied. Figures 6 a-c report the diffuse reflectance UV-vis spectra (DRS) of pure TiO_2 and PMo_{12}/TiO_2 with different contents of PMo_{12}, calcination temperatures and times. The optical absorption edge and band gap values of different prepared photocatalysts were collected in Table 2. For pure TiO_2, the broad intense absorption edge from ~400 nm to lower wavelengths region is associated with the intrinsic band gap absorption of the TiO_2 in which

Ti is present as a tetrahedral Ti (IV) (Figure 6a). This absorption band is generally associated with the electronic excitation of the valence band O2p electron to the conduction band Ti 3d level [21]. No separated absorption peak corresponding to PMo_{12} was detected. This result confirmed that the Keggin unit was uniformly dispersed at the atomic level throughout the coupled TiO_2. Compared by the absorption edge wavelength of pure TiO_2 at ~371.9, all PMo_{12} doped TiO_2 observe blue shifts from ~371.9 nm to ~333.2 nm under different preparation conditions, indicating the increasing of the optical band gap (Figure 6a and Table 2) [22, 30-32]. These observations could be related to interaction between PMo_{12} and TiO_2. Moreover, the absorption edge of 0.0050 PMo_{12} doped TiO_2 increased till 450 °C then decreased by increasing the calcination temperatures (Figures 6b, Table 2). Furthermore, the absorption edge of 0.0050 PMo_{12}/TiO_2 calcined at 450°C for 1h has the highest value of absorption edge (Figures 6c, Table 2).

The band gap (E_g) of the prepared nanomaterials with different content of PMo_{12} was estimated by extrapolation of the linear portion of $(\alpha h\nu)^2$ versus photon energy ($h\nu$) plots using the relation [21] $\alpha h\nu = A(h\nu - E_g)^{1/2}$ (2) where $\alpha = 2.303x \ln(I_o/I)/t$, here ln(Io/I), absorbance and t, thickness of the sample. A is a constant for a direct transition and $h\nu$ is photon energy of the incident radiation. Inset of Figures 6 a-c show the $(\alpha h\nu)^2$ vs. ($h\nu$) plot of different nanomaterials. The band gap of pure TiO_2 is 3.04 eV. The different contents of PMo_{12} increased the value of band gap of pure TiO_2. The widening of the TiO_2 band gap energy with the incorporation of PMo_{12} is due to Moss–Burstein effect [14]. The energy difference between the highest level of the valance band and the lowest level of the conduction band is the band gap energy (Eg). When the semiconductor is incorporated with another element, the Fermi

energy level (E_f) lies within the conduction band by certain energy (En). Since the states below the energy E_n are already filled (5d (Mo) and 3d (Ti) orbital), the fundamental transitions to states below $E_g + E_n$ are forbidden. Hence the absorption edge should shift to higher energies by about E_n and consequently the measured band gap is determined from the onset of interband absorption and moves to higher energy or blue shifted. The other important factor to increasing the band gap of the samples is the decrease of the particle sizes with the increasing PMo_{12} loadings may also lead to the change of the band gap of the nanoparticles. The result is confirmed by XRD analysis. The blue shifting of the band gap energy has an enormous impact on the photo-activity of the material. In photocatalysis, the semiconductor becomes more effective when one can minimize the electron– hole recombination. Upon excitation, the electron jumps to conduction band leaving a positively charge hole in the valance band and in an effective photocatalyst more electrons in the conduction band is used for the catalytic activity rather than letting it recombine with the holes in the valence band. In our case, due to the extra energy E_n by which the Fermi energy level E_f is embedded into the conduction band, it somehow inhibits the recombination process and make the electrons available for effective photooxidation process.

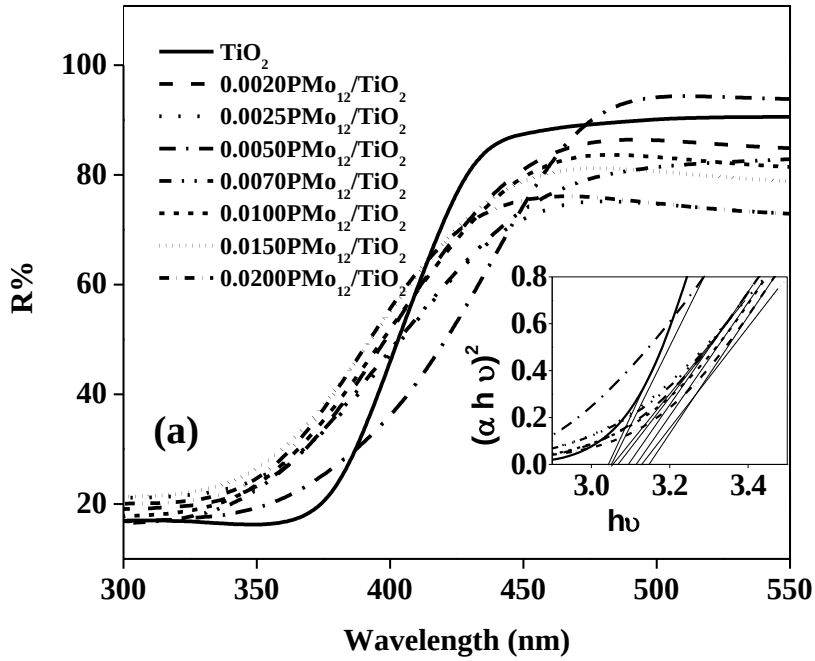
TiO2
0.0020PMo12/TiO2
0.0025PMo12/TiO2
0.0050PMo12/TiO2
0.0070PMo12/TiO2
0.0100PMo12/TiO2
0.0150PMo12/TiO2
0.0200PMo12/TiO2
R%
Wavelength (nm)
(a)
(α h υ)2
hυ

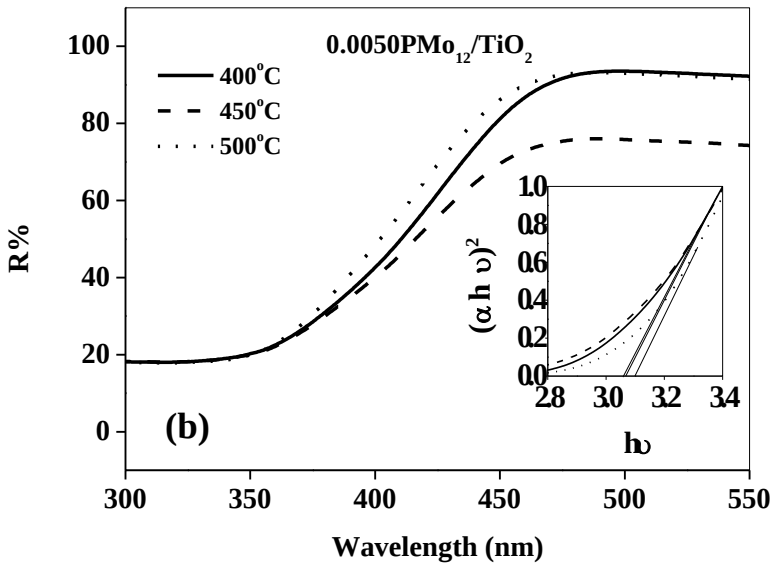
0.0050PMo12/TiO2
400°C
450°C
500°C
R%
Wavelength (nm)
(b)
(α h υ)2
hυ

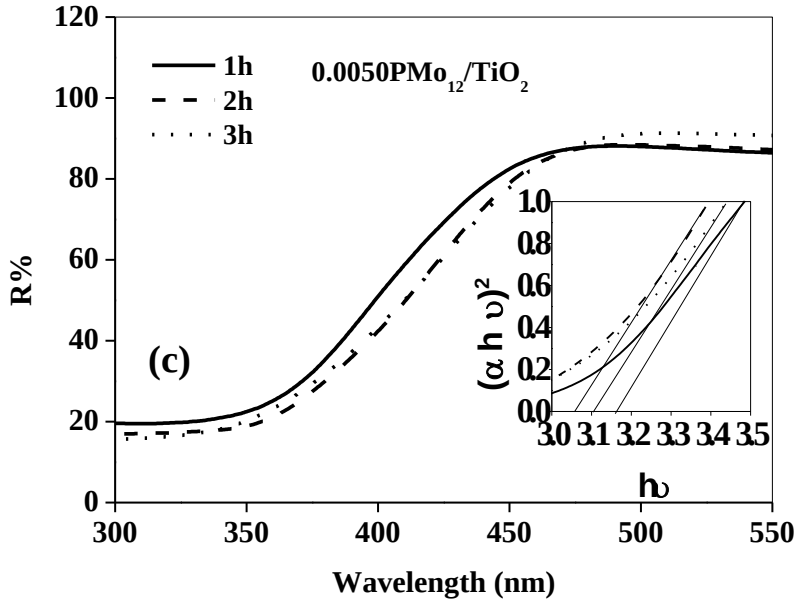

Figure 6: UV-vis/DR spectra of TiO_2 with different contents of PMo_{12} (a), 0.0050 PMo_{12}/TiO_2 at different calcination temperatures (b) and times (c). Inset: plot of $(\alpha h\nu)^2$ versus photonenergy ($h\nu$).

Table 2: Absorption edge and band gap values of TiO_2 and the others chosen PMo_{12}/TiO_2 from UV-Vis spectra analysis.

Conc.	**PMo_{12}/TiO_2**	
	Absorption edge (nm)	Band gap (eV)
0.000 (450°C/1h)	371.91	3.041
0.0020 (450°C/1h)	339.06	3.067
0.0025 (450°C/1h)	341.51	3.055
0.0050 (450°C/1h)	344.10	3.051
0.0070 (450°C/1h)	338.85	3.094
0.0100 (450°C/1h)	337.06	3.114
0.0150 (450°C/1h)	336.31	3.128
0.0200 (450°C/1h)	335.61	3.147
0.0050 (400°C/1h)	333.52	3.067
0.0050 (500°C/1h)	330.01	3.098
0.0050 (450°C/2h)	337.12	3.105
0.0050 (450°C/3h)	333.42	3.160

3.1.5. Photoluminescence properties

The photoluminescence (PL) emission spectra of the TiO_2 in the presence of PM_{12} as a dopant were studied to disclose the separation efficiency of charge carriers, because PL emission results from the recombination of free carrier [9, 14, 21]. Pure TiO_2 exhibited PL emission in blue region (Figure 7). The blue emission was attributed to the recombination of excitons. Slightly blue shift in the emission bands of all PMo_{12} doped TiO_2 samples were observed relative to the pure TiO_2 (Figure 7). This is in line with the observation made by absorption measurements. This indicates that the optical properties of prepared TiO_2 are sensitive to the PMo_{12} doping. Moreover, it can be seen that the PL emission of pure TiO_2 samples was significantly quenched by doping with PMo_{12} (Figure 7). This means that PMo_{12} doping could effectively enhance the separation efficiency of electron – hole pairs by increasing the formation rate of $^{\bullet}OH$ radicals so the photocatalytic activity increased [9, 21].

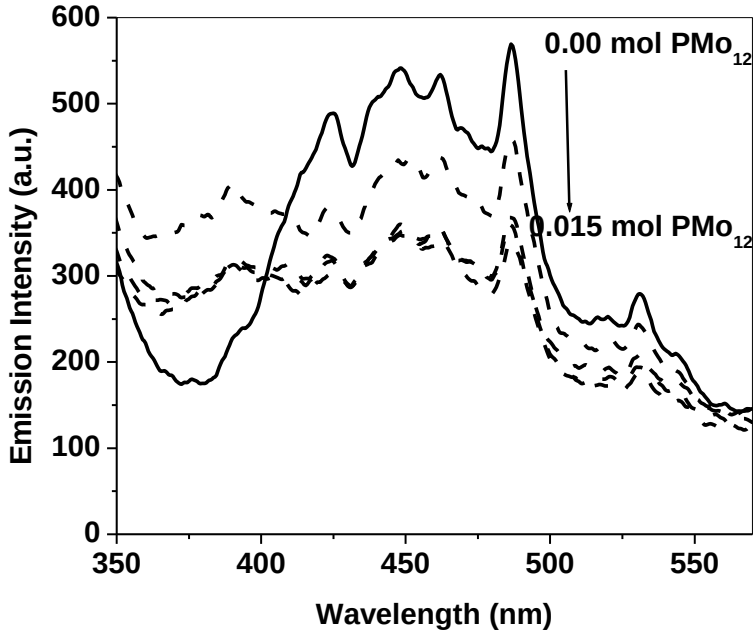

Figure 7: The PL emission spectra of different prepared PMo_{12} doped TiO_2 (λ_{ex} = 325 nm)

3.2. Evaluation methods of photocatalytic activity

3.2.1 Fluorescent probe method

The hydroxyl radicals ($^{\bullet}OH$) generated on the surface of prepared nano-photocatalysts in the semiconductor sensitized advanced photo-oxidation process can be detected by fluorescent probe method using UV irradiation. In this method, a non-fluorescent material (such as Coumarin) is converted to a fluorescent one (7-hydroxycoumarin) using $^{\bullet}OH$ radicals produced within irradiation [33]. Figure 8 presents the increasing of 7-hydroxycoumarin amount by increasing illumination time using 0.0050 PMo_{12} / TiO_2 as model example.

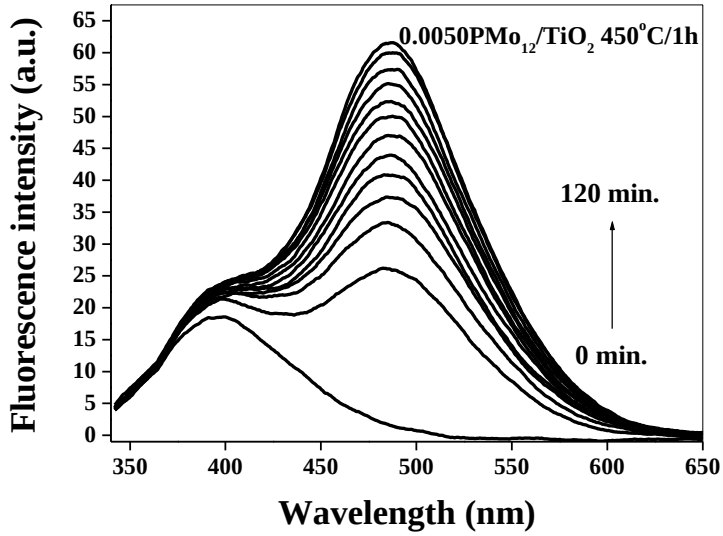

Figure 8: Fluorescence spectral changes of 7-hydroxycoumarin observed during illumination of 0.0050PMo_{12}/TiO_2 at 450 °C /1h immersed in coumarin solution (1.0×10^{-3} M). λ_{ex}= 332 nm.

Graphical relations between the produced 7-hydroxycoumarin fluorescent concentration against illumination time of pure TiO_2 and PMo_{12}/TiO_2 with different contents are presented in Figure 9. 7-hydroxycoumarin concentration was converted from its intensity using the calibration curve, that they are directly proportional to illumination time; achieving the kinetics of pseudo-zero-order reaction rate. The rate constant for photocatalytic oxidation of Coumarin to 7-hydroxycoumarin can be determined from the slope of lines in Figure 9. The rate constant (k_f) of TiO_2 and PMo_{12}/TiO_2 under a varity of conditions (PMo_{12} contents, calcination temperature and calcination time) gained from fluorescent probe method were recorded in Table 3. The increasing of PMo_{12} content enhances the $^{\bullet}OH$ radicals production ability until reach to maximum value for 0.0050 content then decreased. Also from Table 3, it was observed that

the optimum calcination temperature was 450°C and the suitable calcination time was for one hour. The improvement of production of 7-hydroxycoumarin using PMo_{12}/TiO_2 than pure TiO_2 is a result of the reduction of electron / hole recombination rate as seen in the PL study section and this explained as following: the nano-photocatalyst gain photons whose energy higher than that of PMo_{12}/TiO_2's band gap, generating electron-hole pairs. Owing to the synergistic effect between PMo_{12} and TiO_2, the electrons transfer from the conduction band of TiO_2 to PMo_{12}. PMo_{12} accept these electrons and converted to the reduced form (PMo_{12}^-). After that the PMo_{12}^- come back to its original form of HPA by oxidation using O_2 yielding $^{\bullet}O_2^-$ which can form $^{\bullet}OH$ through chain reactions while the reproduced HPA enter another cycle. Holes can react with H_2O to give $^{\bullet}OH$ radicals (eq.3-8) [13, 34].

$$TiO_2 + h\nu \longrightarrow e^- + h^+ \quad (3)$$

$$PMo_{12} + e^- \longrightarrow PMo_{12}^- \quad (4)$$

$$PMo_{12}^- + O_2 \longrightarrow {}^{\bullet}O_2^- + PMo_{12} \quad (5)$$

$$PMo_{12} \longrightarrow \text{recycling} \quad (6)$$

$$^{\bullet}O_2^-(\text{chain reaction}) \longrightarrow {}^{\bullet}OH \quad (7)$$

$$h^+ + H_2O \longrightarrow {}^{\bullet}OH + H^+ \quad (8)$$

Unfourtainatly, the conversion rate of coumarin to 7-hydroxycoumarin decreased after 0.0050 PMo_{12} / TiO_2 due to the presence of anatase phase only so the production of $^{\bullet}OH$ radicals decreased. The presence of anatase and rutile phases in TiO_2 leads to synergistic effect between them, so the electron transfer from conduction band (CB) of one phase to the CB of the other retard the recombination rate between electron and hole.

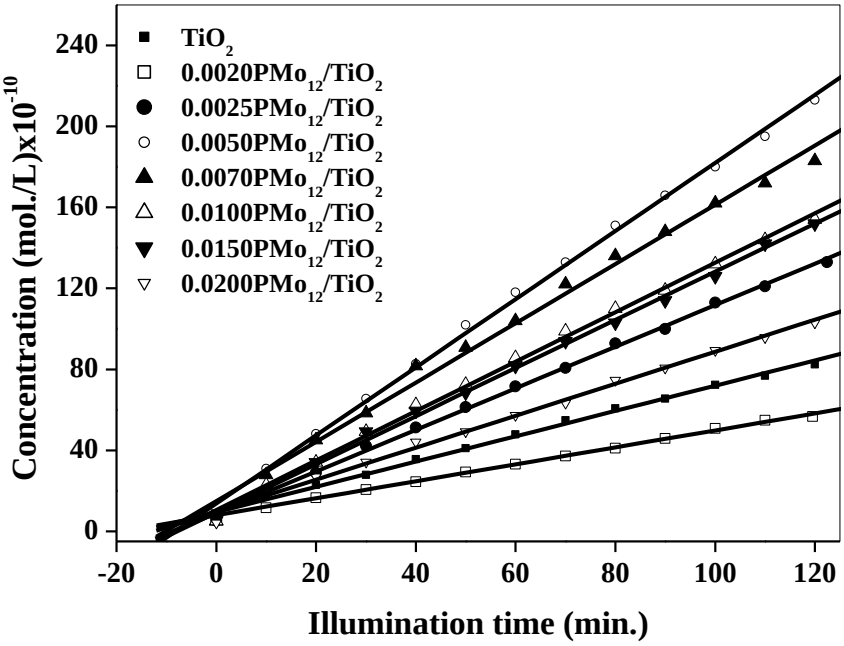

Figure 9: Plots of fluorescence concentration against illumination time for 7-hydroxycoumarin using PMo_{12} /TiO_2 at different contents at 481 nm and (pH=3).

Table 3: The rate constant (k_f) of TiO_2 and PMo_{12}/TiO_2 gained from fluorescent probe method.

Photocatalyst	**PMo_{12}/TiO_2**

	k_1x10^{-10}± Error limit x 10^{-12}	R
TiO_2 (450°C /1h)	0.731±2.58	0.99
0.0020 (450°C /1h)	0.42±0.49	0.99
0.0025 (450°C /1h)	1.04±1.22	0.99
0.0050 (450°C /1h)	1.68±2.64	0.99
0.0070 (450°C /1h)	1.46±3.82	0.99
0.0100 (450°C /1h)	1.22±1.91	0.99
0.0150 (450°C /1h)	1.19±1.75	0.99
0.0200 (450°C /1h)	0.79±1.67	0.99
0.0050 (400°C /1h)	0.95±2.82	0.99
0.0050 (500°C /1h)	1.37±1.37	0.99
0.0050 (450°C /2h)	1.08±2.52	0.99
0.0050 (450°C /3h)	0.66±1.98	0.99

3.2.2 Dye method for evaluation of photocatalytic activity of prepared catalysts

Figure 10 shows that the main absorption peak of RR (513 nm at pH=3) was reduced after 30 min in the presence of 0.0050 PMo_{12}/TiO_2 as the representative example. The comparison of initial decolorization rates (K) of RR using the prepared PMo_{12}/TiO_2 with different PMo_{12} contents from 0.0050 to 0.0200 were shown in Figure 11. Pure TiO_2, 0.0020 PMo_{12}/TiO_2 and 0.0025 PMo_{12}/TiO_2 were found that have adsorption behavior not photoctalytic one. The experimental data (rate constants and decolorization efficiency) of the mesoporous nanoparticles estimated using first order kinetic equation: Ln

$(A/A_o) = - kt$ are shown in Table 4. Where A_o and A are the concentration of the absorbance of RR solution at UV light irradiation time of t= 0 and t, respectively [33, 35, 36]. Table 4 and Figure 11 shows that, the values of k and decolorization efficiency of 0.0050 PMo_{12}/TiO_2 have the maximum values compared to the each series separately. By increasing doping content, the value of k decreases as a result the decolorization efficiency decreased. Also, by increasing the calcinations temperature, the rate constant increases until 450°C then decreased (Table 4). On the other hand, we found the highest rate constant and decolorization efficiency in case of 1 h calcinations time (Table 1).

Two general factors play important functions to improve the photocatalytic activity of nano-particles. The first one is catalytic factor that include the effects of crystal size, surface area and morphology of the particles. The second one was the photo-factor such as band gap, formation of $^{\bullet}OH$ radicals and synergistic effect between different polymorphs. Although 0.0050 PMo_{12}/TiO_2 calcined at 450°C for one hour has small surface and large crystal size, it has the highest photocatalytic activity. This is due to owing high ratio between rutile and anatase (synergistic effect), small band gap and high $^{\bullet}OH$ radicals production as shown from XRD, UV-vis/DR and Fluorescent probe method. By increasing the concentration of PMo_{12} than 0.0050 the photocatalytic activity decreased and this is a result of the disappearance of rutile compared to that of anatase, increasing the band gap and consequently low $^{\bullet}OH$ radicals production. 0.0050PMo_{12}/TiO_2 (450˚C/1h) has the highest photocatalytic activity comparing by the others that prepared in different conditions due to presence both anatase and rutile phases and this means high separation between electron and hole.

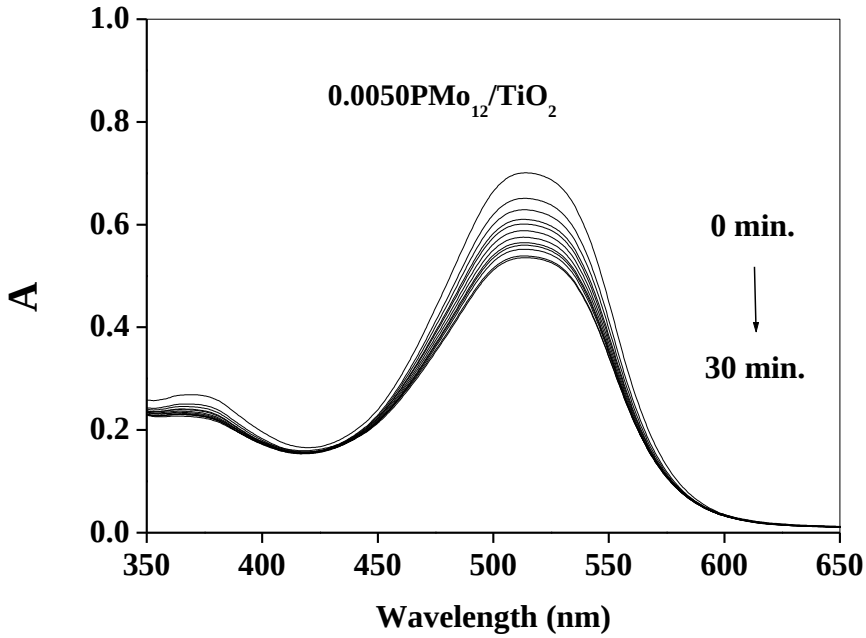

Figure 10: The UV-Vis spectra of RR in acidic aqueous medium (pH=3) at different UVA irradiation times intervals of 0.0050 PMo_{12}/TiO_2 at 450 °C /1h.

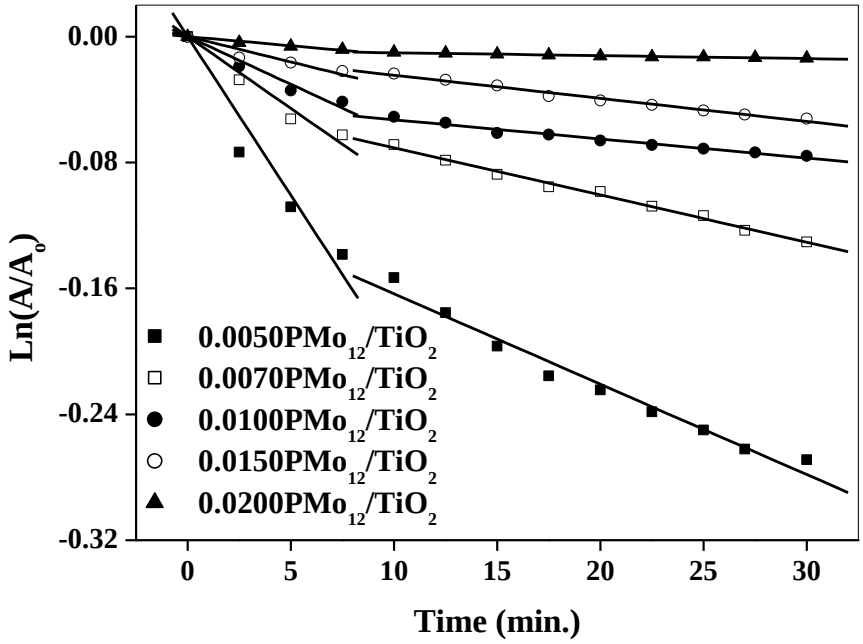

Figure 11: The decolorization rates of RR (5 x 10^{-5} M) using TiO_2 at different contents of PMo_{12}.

Table 4: Rate constants and decolorization efficiency of RR dye degradation from dye method by TiO_2 and PMo_{12}/TiO_2.

Photocatalyst	PMo_{12}/TiO_2				
	First rate		Second rate		Decolorization %
	k_1x10^{-3}± error limit x 10^{-4}	R	k_1x10^{-4}± error limit x 10^{-5}	R	
TiO_2	-	-	-	-	-
0.0020	-	-	-	-	-
0.0025	-	-	-	-	-
0.0050	**-20.2 ± 16.9**	**0.97**	**-57.1 ± 35.7**	**0.98**	**23.57**
0.0070	**-9.13 ± 6.26**	**0.98**	**-30.1 ± 9.69**	**0.99**	**12.23**
0.0100	**-6.06 ± 4.18**	**0.98**	**-12.2 ± 7.44**	**0.98**	**6.98**
0.0150	**-3.22 ± 3.58**	**0.95**	**-14.7 ± 7.07**	**0.98**	**5.08**
0.0200	**-1.17 ± 0.74**	**0.98**	**-1.84 ± 1.35**	**0.98**	**0.71**
0.0050 400°C/1h	**-16.01 ± 14.0**	**0.97**	**-30.4 ± 25.28**	**0.97**	**8.44**
0.0050 500°C/1h	**-14.7 ± 15.1**	**0.96**	**-33.4 ± 18.5**	**0.98**	**15.23**
0.0050 450°C/2h	**-15.2 ± 16.4**	**0.96**	**-26.1 ± 20.2**	**0.97**	**15.34**

References

[1] Environmental Protection Agency, Handbook Advanced Photochemical Oxidation Processes, United States, Washington, DC 20460, December (1998).

[2] M. Izadifard, G. Achari and C. H. Langford, Application of Photocatalysts and LED Light Sources in Drinking Water Treatment, Catal. 3 (2013) 726-743.

[3] G. Marcì, E. García-López and L.Palmisano, Photo-assisted degradation of 2-propanol in gas–solid regime by using TiO_2 impregnated with heteropolyacid $H_3PW_{12}O_{40}$, Catal.Tod. 144 (2009) 42–47.

[4] K. Zhaoa, Y. Lua, N. Lua, Y. Zhaoa, X. Yuana, H. Zhang, L. Tenga and F. Li, Design of $H_3PW_{12}O_{40}/TiO_2$nano-photocatalyst for efficient photocatalysis under simulated sunlight irradiation, Appl. Surf. Sci. 285P (2013) 616-624.

[5] M. Luo, K. Cheng, W. Weng, C. Song, P. Du, G. Shen, G. Xu and G. Han, Preparation of high-density TiO_2nanodots on Si substrate by a novel method, Mater. Lett. 62 (2008) 1965–1968.

[6] M. A. Lazar, S. Varghese and S. S. Nair, Photocatalytic Water Treatment by Titanium Dioxide: Recent Updates, Catal. 2 (2012) 572-601.

[7] N. Lua, Y. Zhaoa, H. Liub, Y. Guoa, X. Yuana, H. Xua, H. Penga and H. Qina, Design of polyoxometallate–titania composite film ($H_3PW_{12}O_{40}/TiO_2$) for the degradation of an aqueous dye Rhodamine B under the simulated sunlight irradiation, J. Hazar. Mater. 199– 200 (2012) 1– 8.

[8]D. A. H. Hanaor and C. C. Sorrell, Review of the anatase to rutile phase transformation, J. Mater. Sci. 46 (2011) 855–874.

[9] M.Saif, S.A.El-Molla, S.M.K.Aboul-Fotouh, H.Hafez, M.M.Ibrahim, M.S.A.Abdel-Mottaleb and L.F.M.Ismail, Synthesis of highly active thin film based on TiO_2 nanomaterial for self-cleaning application, Spectrochimic. Acta A, 112 (2013) 46-51.

[10] G. S. Mital and T. Manoj, A review of TiO_2 nanoparticles, Chin. Sci. Bull. 56 (2011) 1639–1657.

[11] Z. Xiong, H. Wu, L. Zhang, Y. Gu and X. S. Zhao, Synthesis of TiO_2 with controllable ratio of anatase to rutile, J. Mater. Chem.A 2 (2014) 9291- 9297.

[12] L. Xua, G. Wangb, F. Maa, Y. Zhaoc, N. Luc, Y. Guoa and X. Yangc, Photocatalytic degradation of an aqueous sulfamethoxazole over the metallic silver and Keggin unit codopedtitanianocomposites, Appl. Surf. Sci. 258 (2012) 7039– 7046.

[13] W. Choi, A. Termin and M.R. Hoffmann, The role of metal ion dopants in quantum-sized TiO_2: correlation between photoreactivity and charge carrier recombination dynamics, J. Phys. Chem. 98 (1994) 13669–13679.

[14] M. Saif, H. Hafez, A.I. Nabeel, Photo-induced self-cleaning and sterilizing activity of Sm^{3+} doped ZnO Nanomaterials, Chemosphere 90 (2013) 840–847.

[15] O. Akhavan, Thickness dependent activity of nanostructured TiO_2/α-Fe_2O_3photocatalyst thin films, Appl. Surf. Sci. 257 (2010) 1724–1728.

[16] S. Zhang, L. Chen, H. Liu, W. Guo, Y. Yang, Y. Guo and M. Huo, Design of $H_3PW_{12}O_{40}/TiO_2$ and $Ag/H_3PW_{12}O_{40}/TiO_2$ film-coated optical fiber photoreactor for the degradation of aqueous rhodamine B and 4-nitrophenol under simulated sunlight irradiation, Chem. Eng. J. 200–202 (2012) 300–309.

[17] L. Wang, X. Fu, Y. Han, E. Chang, H. Wu, H. Wang, K. Li and X. Qi, Preparation, Characterization, and Photocatalytic Activity of TiO_2/ZnO nanocomposites, J. Nanomater. 2013 (2013) 1-6.

[18] Q. Xiao, Z. Si, J. Zhang, C. Xiao and X. Tan, Photoinduced hydroxyl radical and photocatalytic activity of samarium-doped TiO_2nanocrystalline, J. Hazard. Mater. 150 (2008) 62–67.

[19] S. Asal, M. Saif, H. Hafez, S. Mozia, A. Heciak, D. Moszyński and M. S. A. Abdel-Mottaleb, Photocatalytic generation of useful hydrocarbons and hydrogen from acetic acid in the presence of lanthanide modified TiO_2, Int. J. Hydrog. Energy 36 (2011) 6529-6537.

[20] F. Changgen, X. Gang and L. Xia, Photocatalytic degradation of imidacloprid by composite catalysts $H_3PW_{12}O_{40}$/La-TiO_2, J. Rare Earths 31 (2013)44-48.

[21] M. Saif, S. M. K. Aboul-Fotouh, S. A. El-Molla, M. M. Ibrahim and L. F. M. Ismail, Improvement of the structural, morphology, and optical properties of TiO_2 for solar treatment of industrial wastewater, J. Nanopart. Res. 14 (2012) 1227

[22] J. Li, W. Kang, X. Yang, X. Yu, L. Xu, Y. Guo H. Fang and S. Zhang, Mesoporoustitania-based $H_3PW_{12}O_{40}$ composite by a block copolymer

surfactant-assisted templating route: Preparation, characterization, and heterogeneous photocatalytic properties, Desalination 255 (2010) 107–116.

[23] S. Islama, R. A. Rahmana, S. Riazc, S. Naseemc and Z. Ottomanb, Formation of rutile titania phase at low temperature, Mater. Today: Proc. 2 (2015) 5298 – 5301.

[24] S. M. Kumbar, G.V. Shanbhag, F. Lefebvre and S.B. Halligudi, Heteropoly acid supported on titania as solid acid catalyst in alkylation of *p*-cresol with *tert*-butanol, J. Mol. Catal. A: Chem. 256 (2006) 324–334.

[25] K. Li, Y. Guo, F. Ma, H. Li, L. Chen, Y. Guo, Design of ordered mesoporous $H_3PW_{12}O_{40}$-titania materials and their photocatalytic activity to dye methyl orange degradation, Catalysis Communications 11 (2010) 839–843.

[26] K. Li, X. Yanga, Y. Guoa, F. Maa, H. Li, L. Chena and Y. Guoa, Design of mesostructured $H_3PW_{12}O_{40}$–titania materials with controllable structural orderings and pore geometries and their simulated sunlight photocatalytic activity towards diethyl phthalate degradation, Appl. Catal., B 99 (2010) 364–375.

[27] R. A. Spurr and H. Myers, Quantitative Analysis of Anatase-Rutile Mixtures with an X-Ray Diffractometer, Anal. Chem. 29 (1957) 760-761.

[28]X. Yana, P. Meia, J. Lei, Y. Mia, L. Xionga, and L. Guob, Synthesis and characterization of mesoporousphosphotungstic acid/TiO_2nanocomposite as a novel oxidative desulfurization catalyst, J. Mol. Catal. A: Chem. 304 (2009) 52–57.

[29] F. F. Bamoharram, Vibrational Spectra Study of the Interactions Between KegginHeteropolyanions and Amino Acids, Molecules 14 (2009) 3214-3221.

[30] L. Xua, X. Yanga, Y. Guoc, F. Mac, Y. Guoc, X. Yuana, and M. Huoa, Simulated sunlight photodegradation of aqueous phthalate esters catalyzed by

the polyoxotungstate/titanianocomposite, J. of Hazard. Mater. 178 (2010) 1070–1077

[31] N. Pugazhenthiran, S. Ramkumar, P. S. Kumar, and S. Anandan, In-situ preparation of heteropolytungstic acid on TiMCM-41 nanoporous framework for photocatalytic degradation of textile dye methyl orange, MicroporousMesoporous Mater. 131 (2010) 170–176

[32] J. Yu, H. Yu, B. Cheng, M. Zhou and X. Zhao, Enhanced photocatalytic activity of TiO_2 powder (P25) by hydrothermal treatment, J. Mol. Catal. A: Chem. 253 (2006) 112–118.

[33] M. M. Ibrahim and S. Asal, Physicochemical and photocatalytic studies of Ln^{3+}- ZnO for water disinfection and wastewater treatment applications, J. Mol. Struct. 1149 (2017) 404-413.

[34] N. Lu, Y. Lu, F. Liu, K. Zhao, X. Yuan, Y. Zhao, Y. Li, H. Qin, and J. Zhu,$H_3PW_{12}O_{40}/TiO_2$ catalyst-induced photodegradation of bisphenol A (BPA): Kinetics, toxicity and degradation pathways, Chemosphere 91 (2013) 1266–1272.

[35] F. Chang-gen, and S. Hai-ru, Hydrothermal Synthesis of $H_3PW_{12}O_{40}/TiO_2$ Nanometer Photocatalyst and Its Catalytic Performance for Methyl Orange, Chem. Res. Chinese Universities 28(3) (2012) 366—370.

[36] M. A. Zanjanchi, H. Golmojdeh and M. Arvand, Enhanced adsorptive and photocatalytic achievements in removal of methylene blue by incorporating tungstophosphoric acid–TiO_2 into MCM-41, J. Hazard. Mater. 169 (2009) 233–239.